Rupture directivity effects during the April 15, 2016 Kumamoto Mw7.0 earthquake in Japan

Junju Xie[1], Paolo Zimmaro [2], Xiaojun Li[1*], Zengping Wen [1]

1 Institute of Geophysics, China Earthquake Administration, Beijing 100081, China.

2 Department of Civil and Environmental Engineering, University of California Los Angeles, 5731 Boelter Hall, 90095-1593

[*] Also at Beijing University of Technology, Beijing 100124, China.

ABSTRACT

The M_w 7.0 Kumamoto earthquake (Japan) occurred on 15 April 2016 – 16:25 UTC. This earthquake struck approximately 1 km west-northwest of Kumamoto, Japan. We analyze ground accelerations recorded by 136136 near-field stations. We investigate spatial distribution of the recorded ground motions, as well as rupture directivity effects on various intensity measures. We develop a simplified ground motion model that includes both geometric and anelastic attenuation terms. Comparisons of observed and predicted ground motions suggest that, predictions from the NGA-West2 models, provide good fits for the overall observation. In the forward direction, rupture directivity increases ground shaking intensity levels, especially, but not only for long periods. Rupture directivity effects are negligible at locations close to the epicenter. Analysis of spatial distribution of the residuals shows that observed ground motions in the azimuth range 0-30 °along the opposite side of the fault rupture direction (southwest of the fault) can be as low as 0.5-0.9 times the average. Ground motions on the northeast side of the fault in the forward direction are much higher than average, with peak velocity and long-period spectral accelerations ranging from 1.3-1.7 times the average. We also perform a log-linear regression of the residuals, developed using a new directivity predictor. Our results show that for the 2016 M_w 7.0 Kumamoto earthquake, rupture directivity produce significant amplification and deamplification effects in the rupture forward and backward region respectively, particularly for PGV andlong-period spectral acceleration at 3.0s, but no systematic influence are shown on PGA and short periods less than 0.5s.

INTRODUCTION

On 15 April 2016, 16:25 UTC, an earthquake of magnitude M_w 7.0 struck Higashi Ward in the city of Kumamoto (2010 population: ~731,000) – Kyushu region in southwest Japan. Significant damages have been experienced in the following prefectures: Kumamoto, Oita, Fukuoka, Yamaguchi, Saga, Nagasaki, and Miyazaki. The prefecture of Kumamoto has experienced the worst consequences, with over 50,000 buildings damaged, among them, more than 2,400 have totally collapsed, according to the prefectural government. Various seismically-induced ground failure mechanisms occurred in this prefecture (i.e. landslides, liquefaction, surface fault

rupture); also fire-following earthquake has been reported. Important lifelines have been affected by the earthquake, including power, water, and gas systems. At least 66 fatalities and over 1,500 injuries have been reported. Early estimates of the economic costs of the damage range from $5.5 billion to $7.5 billion, with insured property losses estimated to be between $800 million and $1.2 billion.

The Kumamoto main shock was well-recorded by K-NET and KiK-net, two strong motion networks in Japan operated by the National Research Institute for Earth Science and Disaster Resilience (NIED). According to NIED, over 690 groups of three-component accelerograms were recorded by triggered strong motion stations. A large number of digital strong motion recordings are available in the near-fault region. Over 75 groups of accelerograms were recorded by stations located within 60 km of the Futagawa fault. The largest PGA is 1157 cm/s^2 in the E-W direction. It was recorded by the KMMH16 station (Figure 1), close to the epicenter. These near-fault recordings provide an invaluable opportunity for studying rupture directivity effects.

A total of 136 groups of three-component acceleration recordings are used to investigate the rupture directivity effects on strong motion during the Kumamoto M_w 7.0 earthquake. These records are examined and compared with estimations from the NGA-West2 models, based on global database (Ancheta et al., 2014). We then investigate spatial variability and rupture directivity effects on near-fault strong motion using residual analysis. Based on these results, we present a quantitative directivity model for this event which includes a new directivity predictor. We anticipate that results from this study will be useful for future GMMs development, as well as for a broader improvement of the technical knowledge on directivity effects for large shallow crustal earthquake events.

STRONG MOTION DATA

The strong motion dataset used in this study consists of three-component accelerograms recorded by the NIED strong-motion seismograph networks of Japan. These data are available in a unified website for both K-NET and KiK-net networks. Figure 1 shows the 136 stations used in this study. The selected stations are all located within 100 km of the finite fault plane of the Kumamoto M_W 7.0 earthquake. For KiK-net stations, we only use three-component recordings observed on the ground surface, because intensity measures (IMs) recorded by downhole accelerometers are usually lower than those recorded on the surface, and ground motion models (GMMs) are developed using data observed on ground surface from free-field stations. All selected recordings from K-NET and KiK-net are sampled at 100S/sec.

The K-NET and KiK-net unified website also provides soil profile data at strong motion station locations. The sites are classified based on the time-averaged shear wave velocity in the upper 30 m (V_{S30}). For K-NET stations with soil profile depth less than 30 m we use a V_{SZ}-to-V_{S30} extrapolation model for Japan (Boore et al., 2011) to calculate V_{S30}. Source-to-site distances for each station are calculated using the earthquake source geometry (Figure 1) provided by USGS (2016). To avoid missing displacement information after high-pass filtering, and recover reliable permanent displacements, we process the records using a modified version of the

multi-consecutive-segment baseline correction method (e.g. Boore, 2001; Akkar and Boore, 2009), initially proposed by Iwan et al. (1985).

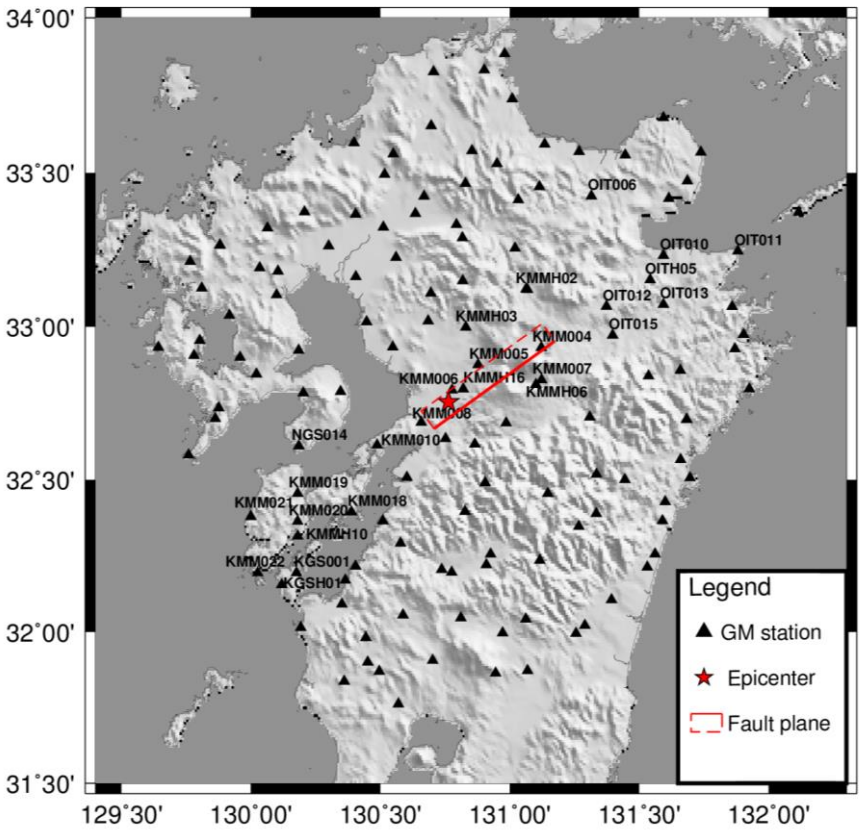

Figure 1 Location of strong motion stations used in this study, along with the ruptured finite fault plane of the Kumamoto M_W 7.0 earthquake (Yagi et al., 2016).

COMPARISON OF OBSERVED HORIZONTAL GROUND MOTION WITH NGA-WEST2 GROUND MOTION MODELS (GMMS)

The intensity measures (IMs) used in this study, are peak ground acceleration and velocity, PGA and PGV; and spectral acceleration (SA) at various periods. We define them as the geometric mean of PGAs, PGVs and SAs of the two as-recorded horizontal (EW and NS) components of the ground motion. In this section, we compare variation of the horizontal ground motion intensity measures with distance, observed during the Kumamoto main shock, with predictions from the NGA-West2 GMMs. All these analyses are performed using the closest distance to the rupture plane R_{rup} as source-to-site distance. The observed data are adjusted to a common velocity using the Seyhan and Stewart (2014) model (hereafter SS14, which represents the site term in the Boore et al., 2014 model) in which amplitude and frequency-dependent site effects are a function of V_{S30}, relative to a reference site condition (i.e. 760 m/s).

Based on strong motion data introduced in the previous section, we develop an *ad hoc* simplified GMM, that includes both geometric and anelastic attenuation term, with rupture distance R_{rup}. The functional form, similar to the Campbell and Bozorgnia (2014) model, is given as:

$$\ln(Y) = a + b \cdot \ln\left(\sqrt{R_{rup}^2 + c^2}\right) + d \cdot R_{rup} + \sigma_{\ln(Y)} \quad (1)$$

where Y represents the observed IM, and coefficients a, b, c, and d are derived from regression analysis performed using the least squares method; $\sigma_{\ln(Y)}$ is the standard deviation of the regression.

Figure 2 shows variation of the considered IMs (PGA, PGV, and SA) with R_{rup}, along with least squares regression lines obtained from Equation 1. These results are compared with median predictions from the NGA-West2 models (Abrahamson et al. (2014), ASK14; Campbell and Bozorgnia (2014), CB14; Chiou and Youngs (2014), CY14; and Boore et al. (2014), BSSA14). The predictions from the NGA-West2 models provide a reasonably good fit for the observed data.

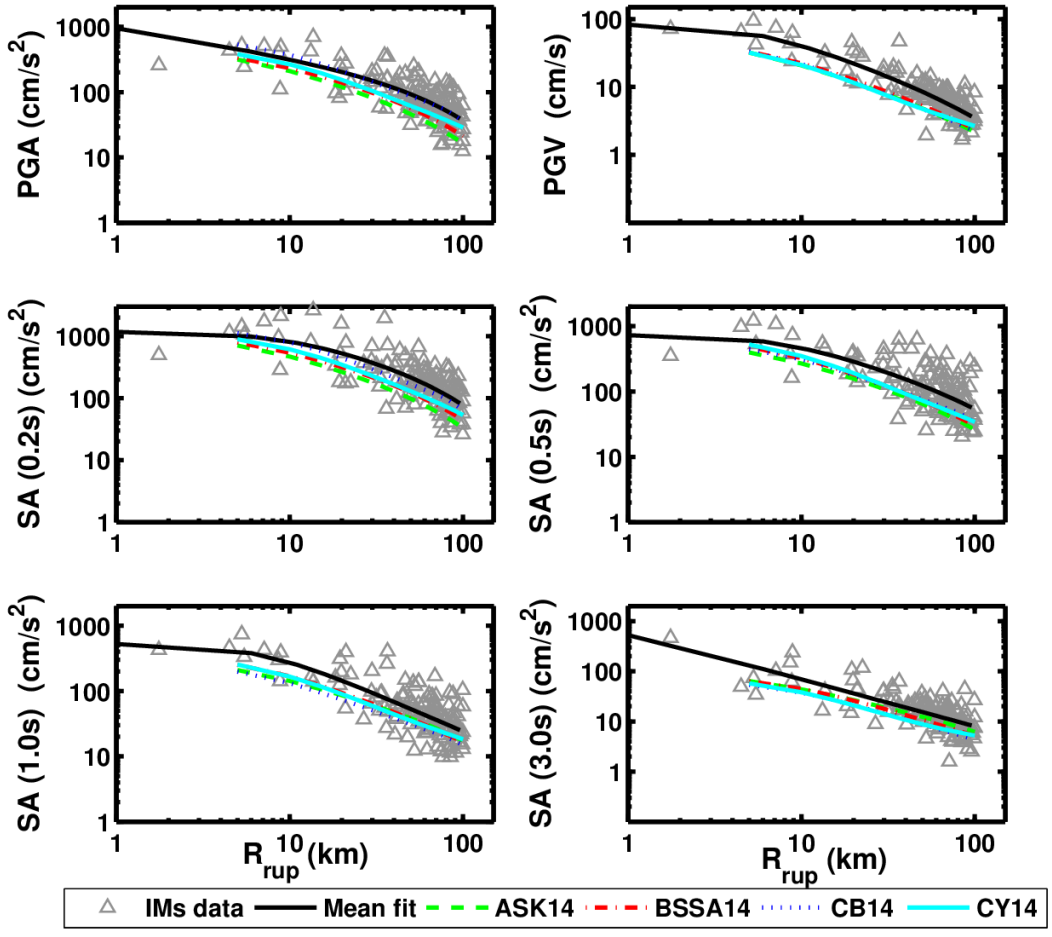

Figure 2 Variation of IMs with R_{rup} and comparison with NGA-west2 models. All observed data are adjusted to site condition of V_{S30} = 760 m/s based on the Seyhan and Stewart (2014) model (SS14). ASK14, CB14, CY14 and BSSA14 indicate median predictions from Abrahamson et al. (2014), Campbell and Bozorgnia (2014), Chiou and Youngs (2014), and Boore et al. (2014) model, respectively. We use V_{S30} = 760 m/s for all NGA-West2 models.

Figures 3 and 4 show observed acceleration spectra in the forward and backward direction of fault rupture respectively along with predicted spectral accelerations

versus period (T) from NGA-West2 models. Location of strong motion stations along with their codes are shown in Figure 1. Figure 3 shows that, in the forward direction mean predictions from NGA-West2 models underestimate observed spectra for long-period ground motions (i.e. T > 2.0 s) at the following stations: KMM004, KMM007, KMMH06, OIT010, and OIT012. Observed spectra at the stationOIT006 are uniformly higher than mean predictions from NGA-West2 models for all periods (0.01-10 s). These results suggest that, in the forward direction, rupture directivity increases ground shaking intensity levels, especially, but not only, for long periods. Stations KMM005, KMM006, and KMMH16 are located close to the epicenter in the forward direction. For these stations, NGA-West2 models provide good predictions, indicating that rupture directivity effects are negligible at these three locations.

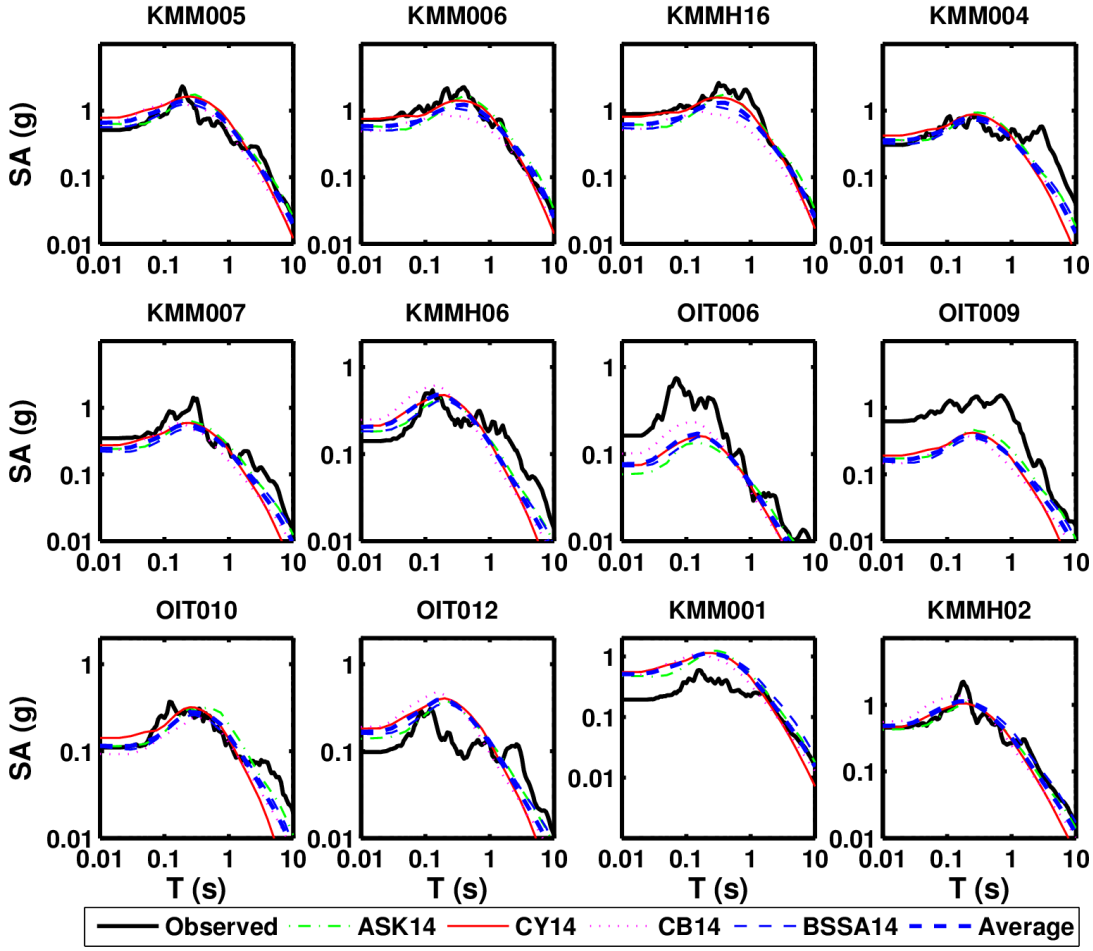

Figure 3 Comparison of observed acceleration spectra in the forward of rupture direction with median predictions from NGA-West2 models. Observed horizontal spectral are calculated from the geometric mean of the as-record EW and NS components. ASK14, CB14, CY14 and BSSA14 indicate median predictions from Abrahamson et al. (2014), Campbell and Bozorgnia (2014), Chiou and Youngs (2014), and Boore et al. (2014) models, respectively. Here different V_{S30} values are assigned from site to site in ASK14, CB14, CY14 and BSSA14 models. Thick blue dashed lines ('Average') represent average prediction of the ASK14, CB14, CY14 and BSSA14 models.
I will update figure 3 and 4 very soon.

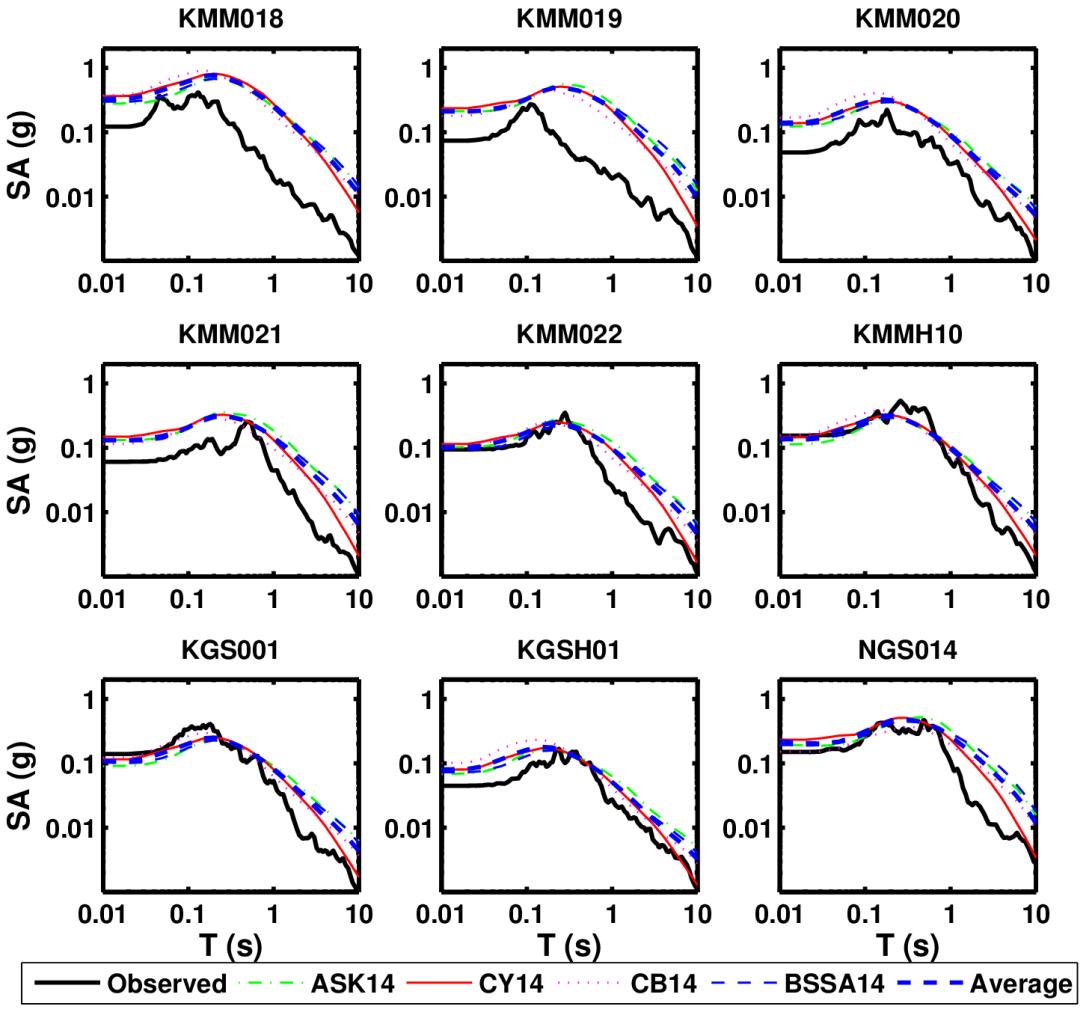

Figure 4 Same as Fig. 3 but for stations located in the backward rupture direction.

Figure 4 shows that NGA-West 2 models predictions, overestimate observed spectra at stations KMM018, KMM019, KMM020, KMM021, and KGSH01 (in the backward direction) for all periods. Observed spectra at the following stations: KMM022, KMMH10, KGS001, and NGS014 are lower than those predicted by the NGA-West2 models, for long-period ground motions (T > 2.0 s).

SPATIAL VARIABILITY OF OBSERVED GROUND MOTIONS AND AZIMUTHAL VARIATION EFFECTS

Previous studies have shown that near-fault ground motion is significantly influence by the focal mechanism and rupture process of causative fault (e.g. Somerville et al., 1997; Bradley and Cubrinovski, 2011; Xie et al., 2014). In this study, we use residual analysis for investigating the spatial distribution of observed near-fault strong motion.

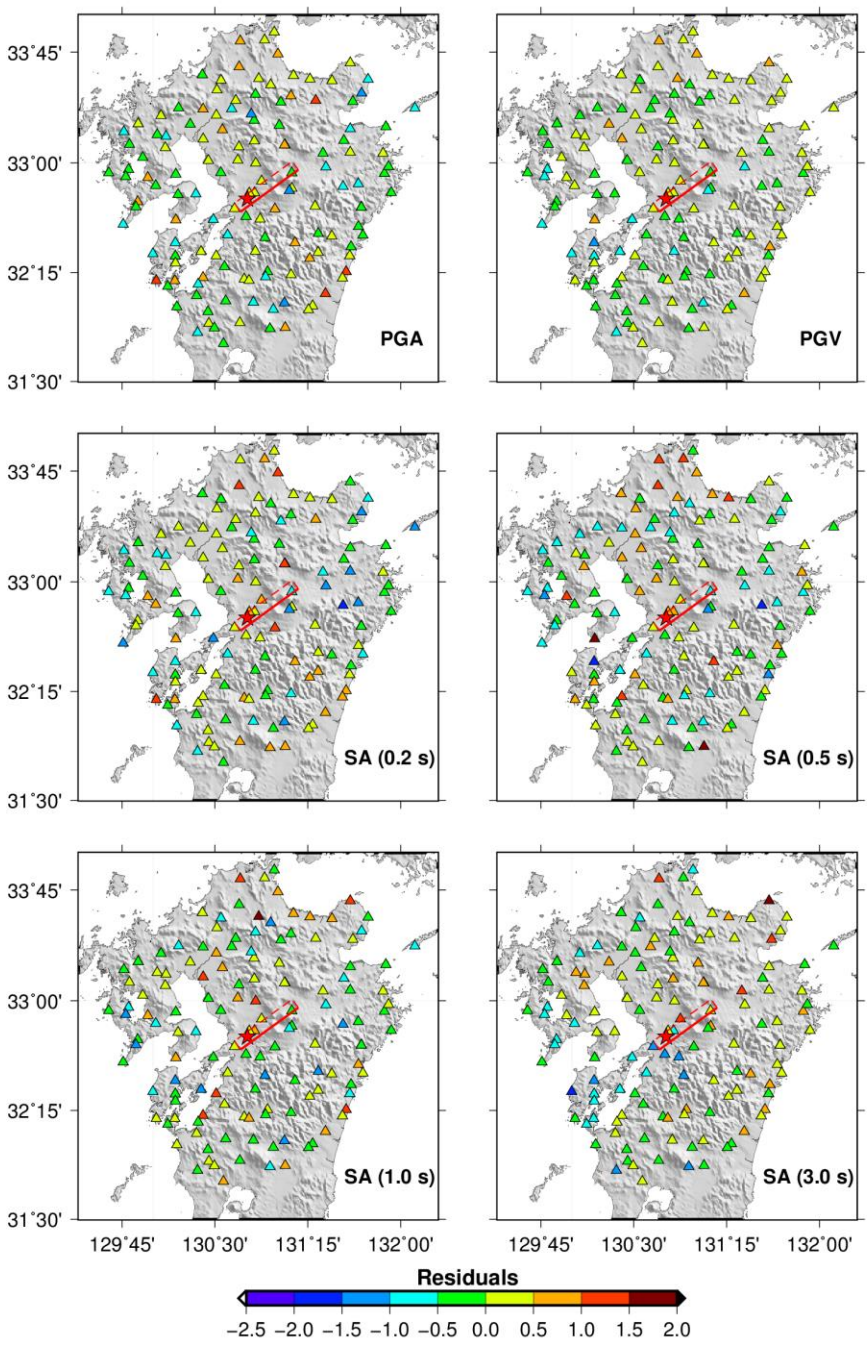

Figure 5 Spatial distribution of residuals (triangles) for various intensity measures, around the causative fault (rectangle).

Figure 5 shows the spatial distribution of residuals for various IMs. The smallest residuals (-2.0 to -2.5) are located southwest of the causative fault. Thus, ground motions observed on the opposite side of the rupture direction are significantly lower than the average values. Ground motions on the northeast side of the fault, are higher than average, with largest residuals equal to 2.0. In particular, the residuals of PGV and spectral acceleration at 3s exhibit clear directivity amplification in the rupture forward region, but those at PGAs and short periods do not. The observed characteristics of residuals spatial distribution are consistent with those observed during the 2008 M_w 7.9 Wenchuan and 2014 South Napa earthquake (Wen et al., 2010;

Baltay and Boatwright, 2015).

Directivity effects are inherently related to systematic azimuthal variations in the strong motion amplitude residuals. In the remainder of this section, we investigate the variation of strong motions with azimuth angles between fault plane and ray path to observation locations. Our definition of azimuth angle is the same used by Kaklamanos et al. (2011). Figure 6 shows residuals versus azimuth of the observation station sites for various IMs. There is a trend of increasing residuals with increasing azimuths in the range 0-180 °; this trend is evident for PGV and SA (3.0 s). For azimuth angles between -180 ° and 0 °, the residuals increase with decreasing azimuth. For azimuth values between -10 °and 20 °, there are the smallest residuals, while the largest residuals are present for azimuth values of about 180 °, which is the rupture direction of the causative strike-slip fault.

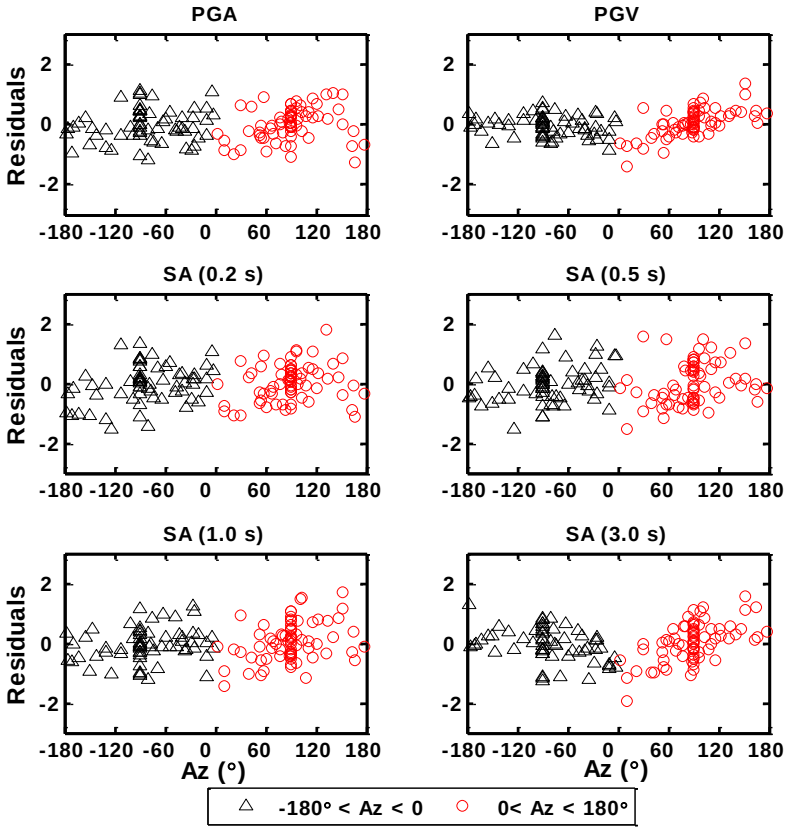

Figure 6 Variation of residuals with azimuth for observed PGA, PGV, and SA at the following periods:0.2 s, 0.5 s, 1.0 s, and 3.0 s. The data with -180° < Az < 0 denote sites in the footwall side of the causative fault, while data with 0 < Az < 180 ° denote sites in the hanging wall side. Note that many data points are clustered at azimuth of ±90°, which indicate sites on the hanging wall and footwall according to the definition of azimuth following Kaklamanos et al. (2011).

Based on the absolute values of azimuth ($|Az|$), we group residual data into 7 bins. Figure 7 shows the variation of mean residuals and standard deviations with azimuth angles. The residuals generally increase with increasing $|Az|$ for PGV and SA (3.0 s); observed PGV and SA (3.0 s) are as low as 0.5-0.9 times the average in the

range $0° \le |Az| < 30°$, and the observation in the range $150° \le |Az| < 180°$ are equal to 1.3-1.7 times the average. These results suggest that rupture directivity has a significant effect on the spatial distribution of near-fault strong motions for this event.

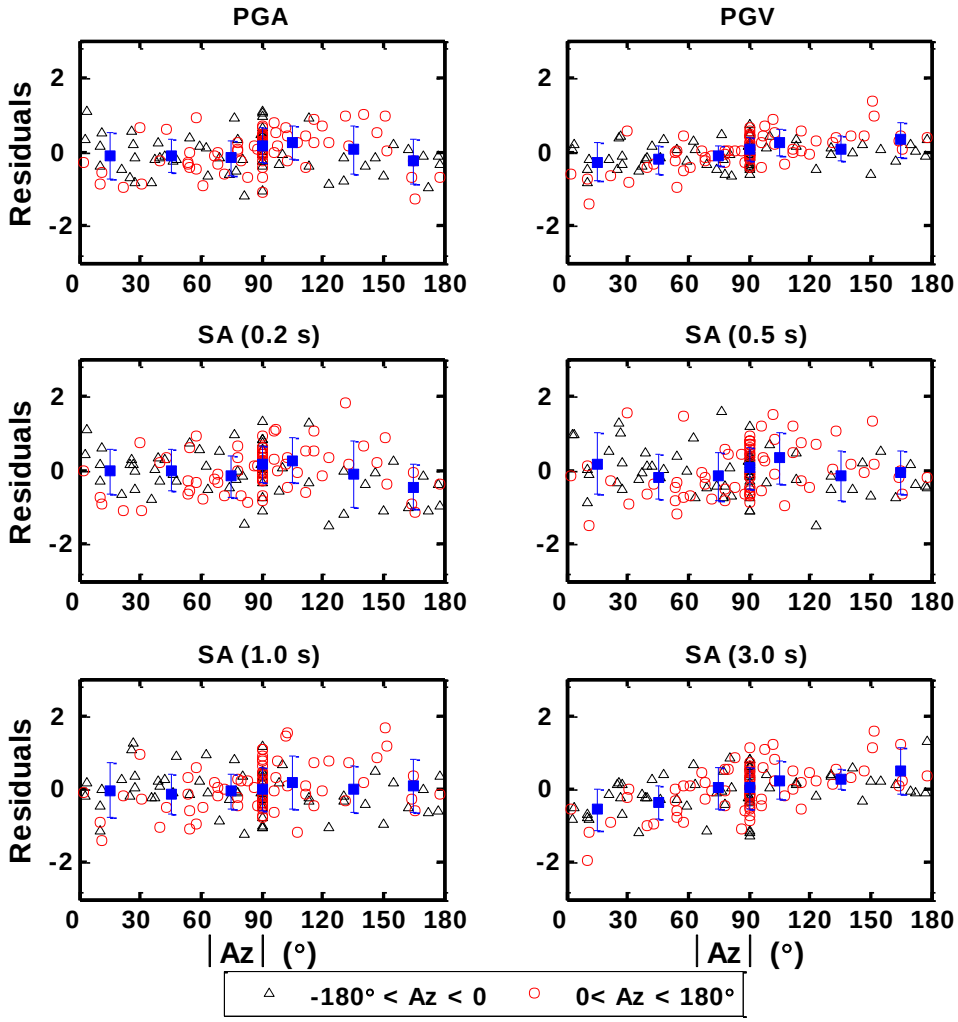

Figure 7 Mean residuals versus observation azimuth for grouped azimuth ranges. The blue square in the center of error bar denote mean residual and the whiskers represent mean ± Std (standard deviation) for each groups.

SUMMARY AND CONCLUSIONS

The 2016 M_w 7.0 Kumamoto earthquake was well recorded by K-NET and KiK-net, strong motion networks in Japan. Over 136 groups of three-component strong motion recordings are available in the near-fault region of the earthquake. This substantial dataset provides invaluable data for the investigation of rupture directivity effects. Although several recent global directivity models are available in the literature, full consensus has not been reached among them (Spudich et al., 2013, 2014).

In this study, we use the substantial dataset from the M_w 7.0 Kumamoto earthquake to investigate the following features: (1) spatial distribution characteristics of the ground motion, and (2) rupture directivity effects on PGA, PGV and spectral acceleration at various periods. The observations are then compared with NGA-West2

GMMs. We find that, for the whole dataset, NGA-West2 models produce good estimation of the attenuation with distance for PGA, PGV and SA at various periods. However, as a result of significant spatial variability induced by rupture directivity during this event, NGA-West2 predictions underestimate long period (i.e. T > 2.0 s) spectral accelerations in the rupture forward direction by a large amount. In the backward direction, NGA-West2 GMMs, consistently overestimate observed spectra for all periods. For stations located close to the epicenter, NGA-West2 models provide good predictions, indicating that rupture directivity effects are practically negligible. Spatial distribution of the residuals shows that on the southwest side of the causative fault (opposite side of the fault rupture direction), observed ground motions are significantly lower than the average. On the northeast side of the fault, residuals are constantly higher than the average, with largest residual values equal to 2.0.

Residual analysis shows that observed ground motions generally increase with $|Az|$, which are as low as about 0.4-0.7 times the average in the range $0° \le |Az| < 30°$. On the other hand, ground motions can be as high as 1.6-1.9 times the average for PGV and SA (3.0 s) in the azimuth range $150° \le |Az| < 180°$. We also perform a log-linear regression of the residuals, developed using a new directivity predictor. The goodness of fit is then evaluated using confidence intervals, determination coefficients, and visual inspection of the data.

DATA AND RESOURCES

The strong motion dataset consists of data recorded by the NIED strong-motion seismograph networks of Japan, available in a unified website for K-NET and KiK-net (http://www.kyoshin.bosai.go.jp/) (last accessed on 10 June 2016). The soil condition data for strong motion stations are also obtained from the same website (last accessed on 20 May 2016). The geophysical maps produced in this study are produced using Generic Mapping Tools (GMT; Wessel and Smith, 1991).

ACKNOWLEDGMENTS

We thank the National Research Institute for Earth Science and Disaster Resilience (NIED) in Japan for providing strong motion data for the Kumamoto M_w 7.0 earthquake. Financial support of this study was fully provided by the National Basic Research Program 973 (2011CB013601) of China, and Natural Science Foundation of China (51578513, 51208476). We also thank professor Jonathan Stewart for his help on the implementation of the Seyhan and Stewart (2014) model.

REFERENCES

Abrahamson, N. A., Silva, W. J., and R. Kamai (2014). Summary of the ASK14 ground motion relation for active crustal regions. *Earthquake Spectra*, **30**(3), 1025-1055.

Akkar, S., and D. M. Boore (2009). On baseline corrections and uncertainty in response spectra for baseline variations commonly encountered in digital accelerograph records. *Bulletin of the Seismological Society of America*, ***99***(3), 1671-1690.

Ancheta, T. D., Darragh, R. B., Stewart, J. P., Seyhan, E., Silva, W. J., Chiou, B. S. J., and T. Kishida (2014). NGA-West2 database. *Earthquake Spectra*, ***30***(3), 989-1005.

Asano, K., and Iwata, T. (2016). Source rupture processes of the foreshock and mainshock in the 2016 Kumamoto earthquake sequence estimated from the kinematic waveform inversion of strong motion data. *Earth, Planets and Space*, **68**(1), 147.

Boore, D. M., Stewart, J. P., Seyhan, E., and G. M. Atkinson (2014). NGA-West2 equations for predicting PGA, PGV, and 5% damped PSA for shallow crustal earthquakes. *Earthquake Spectra*, **30**(3), 1057-1085.

Boore, D. M (2001). Effect of baseline corrections on displacement and response spectra for several recordings of the 1999 Chi-Chi, Taiwan, earthquake. *Bulletin of the Seismological Society of America* **91**(5), 1199-1211.

Boore, D. M., Thompson, E. M., and H. Cadet (2011). Regional correlations of V_S30 and velocities averaged over depths less than and greater than 30 meters. *Bulletin of the Seismological Society of America* **101**(6), 3046-3059.

Bozorgnia, Y., Abrahamson, N. A., Atik, L. A., Ancheta, T. D., Atkinson, G. M., Baker, J. W., Baltay, A., Boore, D. M., Campbell K. W., Chiou, B. S. J., et al. (2014). NGA-West2 Research Project. *Earthquake Spectra* **30**(3), 973-987.

Bradley, B. A., and M. Cubrinovski (2011). Near-source strong ground motions observed in the 22 February 2011 Christchurch earthquake. *Seismological Research Letters*, **82**(6), 853-865.

Campbell, K. W., and Y. Bozorgnia (2014). NGA-West2 ground motion model for the average horizontal components of PGA, PGV, and 5% damped linear acceleration response spectra. *Earthquake Spectra*, **30**(3), 1087-1115.

Chiou, B. S. J., and R. R. Youngs (2014). Update of the Chiou and Youngs NGA model for the average horizontal component of peak ground motion and response spectra. *Earthquake Spectra*, **30**(3), 1117-1153.Gregor, N., Abrahamson, N. A., Atkinson, G. M., Boore, D. M., Bozorgnia, Y., Campbell, K. W., and W. Silva (2014). Comparison of NGA-West2 GMPEs. *Earthquake Spectra*, **30**(3), 1179-1197.

Gallovič, F. (2016). Modeling velocity recordings of the Mw6.0 South Napa, California, earthquake: unilateral event with weak high-frequency directivity. Seism. Res. Lett. 87, 2-14.

Iwan, W. D., Moser, M. A., and C. Y. Peng (1985). Some observations on strong-motion earthquake measurement using a digital accelerograph. *Bulletin of the Seismological Society of America* **75**(5), 1225-1246.

Kaklamanos, J., Baise, L. G., and D. M. Boore (2011). Estimating unknown input parameters when implementing the NGA ground-motion prediction equations in engineering practice. *Earthquake Spectra* **27**(4), 1219-1235.

Koji O. (2016). Earthquake Geology of the April 14 and 16, 2016 Kumamoto Earthquakes.http://119.90.25.34/home.hiroshima-u.ac.jp/kojiok/kumamoto2016 KOreport2.pdf.

Pacor, F., F. Gallovič, R. Puglia, L. Luzi, and M. D'Amico (2016). Diminishing high-frequency directivity due to a source effect: empirical evidence from small earthquakes in the Abruzzo region, Italy. *Geophys. Res. Lett.*, 43, 5000-5008.

Somerville, P. G., Smith, N. F., Graves, R. W., and N. N. Abrahamson (1997). Modification of empirical strong ground motion attenuation relations to include the amplitude and duration effects of rupture directivity. *Seismological Research Letters*, **68**(1), 199-222.

Seyhan, E., and J. P. Stewart (2014). Semi-empirical nonlinear site amplification from NGA-West2 data and simulations. *Earthquake Spectra*,***30***(3), 1241-1256.

Spudich, P., Bayless, J. R., Baker, J. W., Chiou, B. S., Rowshandel, B., Shahi, S. K., and P. Somerville (2013). Final report of the NGA-West2 directivity working group. PEER Report No. 2013/09 Pacific Earthquake Engineering Research Center, UC Berkeley, CA.

Spudich, P., Rowshandel, B., Shahi, S. K., Baker, J. W., and B. S. J. Chiou (2014). Comparison of NGA-West2 directivity models. *Earthquake Spectra*,**30**(3), 1199-1221.

USGS (2016). Preliminary Finite Fault Results for the Apr 15, 2016 M_w 7.0 1 km WSW of Kumamoto-shi, Japan Earthquake (Version 1) http://earthquake.usgs.gov/earthquakes/eventpage/us20005iis#finite-fault.

Wen, Z., Xie, J., Gao, M., Hu, Y., and K. T. Chau (2010). Near-source strong ground motion characteristics of the 2008 Wenchuan earthquake. *Bulletin of the Seismological Society of America*, **100**(5B), 2425-2439.

Xie, J., Li, X., Wen, Z., and C. Wu (2014). Near‐source vertical and horizontal strong ground motion from the 20 April 2013 M_w 6.8 Lushan earthquake in China. *Seismological Research Letters*, **85**(1), 23-33.

Yagi, Y., Okuwaki, R., Enescu, B., Kasahara, A., Miyakawa, A., and M. Otsubo, (2016). Rupture process of the 2016 Kumamoto earthquake in relation with the thermal structure around Aso volcano. *Earth, Planets and Space*, **68**(1), 118.